

Discrete Models for Simulating Surface Growth in 1+1 Dimensions

Kiara Gholizad¹

¹Department of Physics, Sharif University of Technology, Tehran, Iran

April 28, 2025

Abstract

This paper examines discrete simulation models of surface growth like random deposition (RD), relaxed random deposition (RRD), ballistic deposition (BD), and competitive random deposition (CRD) in 1+1 dimensions to explore interface roughness and scaling behavior. We compute scaling exponents (α , β , z) by means of numerical simulations and compare with predictions from stochastic growth equations like Edwards-Wilkinson (EW), Kardar-Parisi-Zhang (KPZ), and Mullins. Our results confirm statistical self-affinity between models with RD with $\beta = 0.50$, RRD in agreement with EW ($\beta \approx 0.23$, $\alpha \approx 0.49$, $z \approx 2.09$), and BD converging towards KPZ universality ($\beta \approx 0.27$, $\alpha \approx 0.38$, $z \approx 1.4$), albeit with deviations reflecting finite-size effects and sensitivity to definition of roughness. CRD varying by angle ($\beta \approx 1.02$ at $\phi = 45^\circ$) and is a consequence of competition between columns. These findings confirm theory while suggesting pragmatic challenges in estimating exponents with implications in surface growth dynamics and material science and other areas.

1 Introduction

Surface growth commonly refers to the buildup of a material interface, as is observed in the formation of crystals or metals. While that context is central to most studies, similar ideas also find use in a range of academic and industrial applications, such as crystal expansion, biological development, and snow layer-

ing. These concepts extend beyond strictly solid materials, appearing in processes like fluid flow through porous media, advancing fire fronts, and bacterial colony expansion.

From a general standpoint, surface growth can be understood as the time evolution of an interface that defines a growing boundary. Empirical evidence shows that such interfaces exhibit common features across a wide variety of growth scenarios. Two notable examples include the way interface roughness evolves over time and the self-affine geometry displayed by many surfaces. Recognizing these shared properties provides strong motivation to investigate surface growth, given its wide relevance in academic research and industrial practice [1]-[8].

In this paper, we focus on modeling different discrete growth processes. In particular, we examine how the roughness of the interface develops and explore scaling behavior across various models. Alongside our simulations, we also discuss several analytical stochastic growth equations commonly studied in the literature. Of particular interest, these equations include Edwards-Wilkinson, Kardar-Parisi-Zhang, and Mullins, each with a different perspective into surface dynamics. By comparison with theoretical benchmarks, our objective is to assess each discrete model's merits and limitations.

We begin by reviewing fundamental principles that illuminate surface growth, including the key definitions and quantities involved in interface growth measurements. We then give a description of stochastic growth equations and how they can be applied to extract scaling and morphological features from sur-

faces. We then outline and apply a variety of discrete simulation methods, with both conceptual benefits and practical limitations. We then give and examine numerical results bridging our discrete models to predictions from analytical methods, and conclude by summarizing our study’s major findings.

2 Background theory

This section describes the underlying theory supporting the study of surface growth. A more complete discussion can be found in references [9, 10], but we reiterate the crucial elements here. We begin with the notions of fractals and self-affinity, then move on to central topics such as interface roughness and scaling exponents. Finally, we introduce several analytical frameworks—the Edwards-Wilkinson (EW), Kardar-Parisi-Zhang (KPZ), and Mullins diffusion equations—that will serve as benchmarks when we interpret the behavior of the discrete growth models presented later.

When viewed at different magnifications, fractal structures maintain their overall morphology. While classical fractals scale uniformly in all directions, many natural interfaces exhibit different scaling factors along different axes; these structures are termed *self-affine*. Surfaces provide a notable example of such behavior: with appropriate scaling, it becomes highly nontrivial to determine whether a given surface snapshot is at low or high magnification. Rather than displaying an exact repeating pattern at all scales, surfaces often show *statistical* self-affinity, meaning their aggregate properties (like roughness or height fluctuations) remain consistent under scale transformations.

Such self-affine behavior can be characterized using specific quantitative measures. One key metric is *surface roughness*, often defined as the standard deviation of the interface height around its mean value. As the interface evolves, its roughness may initially grow with time before saturating, and this pattern can often be represented with simple power-law relations. Consequently, we introduce scaling exponents that describe how roughness depends on both system size and deposition time. These exponents let us clas-

sify a variety of surface-growth models into a small number of universality classes.

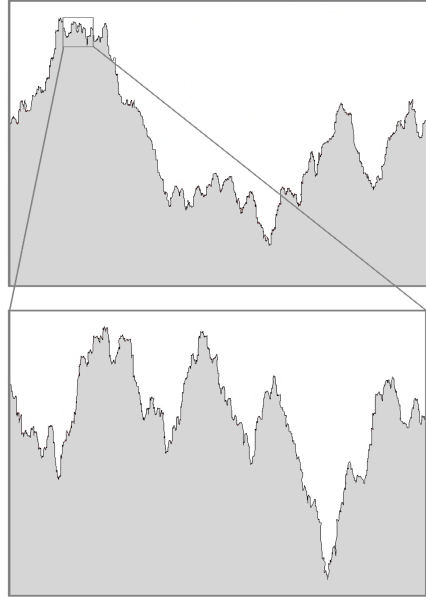


Figure 1: An illustration of a statistically self-affine surface. Without a direct reference, it is nearly impossible to determine the magnification at which the image is captured. Adapted from [11].

Building on this framework, the Edwards-Wilkinson equation adds a linear smoothing term to a stochastic interface, while the Kardar-Parisi-Zhang equation incorporates nonlinear effects associated with growth along local normals. The Mullins equation, for its part, prioritizes curvature-driven diffusion processes that smooth out local height variations more vigorously. Each of these analytical equations predicts distinct scaling exponents. By matching these theoretical forecasts to data produced from discrete simulations, we can determine the key mechanisms driving surface growth in each model.

2.1 Surface roughness and scaling exponents

An important measure in surface growth studies is the *surface roughness*, sometimes termed the *inter-*

face width. It is typically defined as the standard deviation of the surface height distribution at a given time:

$$w(L, t) = \sqrt{\frac{1}{L^d} \sum_{i=1}^{L^d} [h(i, t) - \bar{h}(t)]^2}, \quad (1)$$

where L is the linear dimension of the substrate, d is the spatial dimension (so there are L^d sites), $h(i, t)$ is the height at site i and time t , and $\bar{h}(t)$ is the average height of the entire surface at time t .

For many growing surfaces, the roughness initially increases as a power law in time:

$$w(L, t) \sim t^\beta, \quad (t \ll t_x), \quad (2)$$

where β is the *growth exponent*. After a characteristic *crossover time* t_x , the roughness saturates to a limiting value $w^* = w_{\text{sat}}(L)$, which itself grows with system size L according to

$$w_{\text{sat}}(L) \sim L^\alpha, \quad (t \gg t_x), \quad (3)$$

The exponent α is referred to as the *roughening exponent* and describes how the final (saturated) roughness depends on the system size. The crossover time also follows a power-law scaling with L :

$$t_x \sim L^z, \quad (4)$$

where z is the *dynamic exponent*.

A straightforward way to estimate t_x is shown schematically in Figure 2, where two straight lines—one for the early-time power-law rise in roughness, the other for the flat, saturated regime—are fitted to the curve. Their intersection marks t_x .

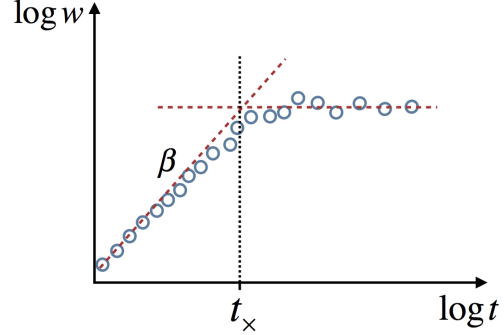


Figure 2: Schematic illustration of how to locate the crossover time t_x : one line describes the initial power-law growth in $w(t)$, while another corresponds to the saturated region. Their intersection identifies t_x .

For different system sizes, plotting $w(L, t)/w_{\text{sat}}(L)$ against t/t_x collapses the roughness curves onto a single universal curve, as exemplified in Figure 3. Here,

$$w_{\text{sat}}(L) \sim L^\alpha, \quad t_x(L) \sim L^z,$$

so the Family-Vicsek scaling relation [?] can be written as

$$\frac{w(L, t)}{w_{\text{sat}}(L)} = f\left(\frac{t}{t_x}\right), \quad (5)$$

where $f(u)$ behaves like u^β for $u \ll 1$ and approaches a constant for $u \gg 1$. Equivalently, one often writes:

$$w(L, t) \sim L^\alpha f\left(\frac{t}{L^z}\right). \quad (6)$$

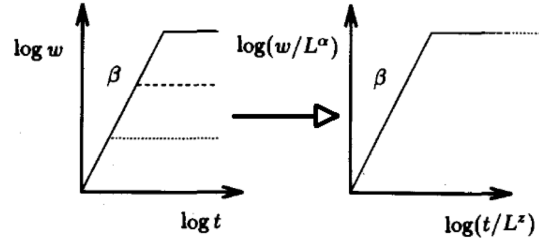


Figure 3: Illustration of roughness curves at several system sizes (top), and how they collapse into a single curve (bottom) upon rescaling by L^α and $t_x \sim L^z$.

From combining these power laws, one also obtains the well-known relation among the exponents:

$$z = \frac{\alpha}{\beta}. \quad (7)$$

Hence, once any two of α, β, z are determined, the remaining exponent follows directly. This simple set of exponents and the corresponding data collapse define a central cornerstone of modern surface growth analyses.

2.2 Stochastic growth equations

Beyond purely numerical approaches, certain surface growth processes can be described by *stochastic continuum* models that allow analytical determination of scaling exponents. These models often take the general form

$$\frac{\partial h(\mathbf{x}, t)}{\partial t} = \Phi(h, \mathbf{x}, t) + \eta(\mathbf{x}, t), \quad (8)$$

where $h(\mathbf{x}, t)$ is the surface height at position \mathbf{x} and time t . The function Φ represents the deterministic part of the growth dynamics, while $\eta(\mathbf{x}, t)$ is a noise term capturing random fluctuations in deposition. Throughout this paper, we concentrate on *Gaussian* noise with no correlations in space or time:

$$\langle \eta(\mathbf{x}, t) \rangle = 0 \quad (9)$$

$$\langle \eta(\mathbf{x}, t) \eta(\mathbf{x}', t') \rangle = 2D \delta^d(\mathbf{x} - \mathbf{x}') \delta(t - t'), \quad (10)$$

where d is the substrate dimension and D a constant related to noise intensity. The precise form of Φ varies with the physical assumptions of each model. Below, we briefly review some of the most common choices.

2.2.1 Random deposition (RD)

The simplest model is *random deposition*, in which incoming particles are dropped vertically at random locations and stick wherever they land, independently of local slopes or heights. In continuous notation, this situation corresponds to a constant growth rate in Φ :

$$\Phi(h, \mathbf{x}, t) = \text{const.}$$

Hence, every site receives incoming particles at the same average rate, with no lateral coupling. Because columns grow independently, the interface never saturates; in effect, there is no correlated smoothing mechanism. One can nonetheless determine the growth exponent β if we regard the system out of equilibrium. From integrating (8) the noise-dominated height evolution, one finds

$$h(\mathbf{x}, t) = Ct + \int_0^t \eta(\mathbf{x}, t') dt', \quad (11)$$

leading to the average height $\langle h(\mathbf{x}, t) \rangle = Ct$. Taking the mean of the square of h and subtracting the square of its mean yields

$$w^2(t) = 2Dt, \quad (12)$$

implying

$$w(t) \sim t^{1/2}.$$

Thus, the roughness exponent for random deposition is

$$\beta = \frac{1}{2}. \quad (13)$$

Since random deposition does not exhibit a finite steady-state roughness, the exponents α and z are undefined in this model.

2.2.2 Edwards-Wilkinson equation

To describe models with correlated lattice sites we need to modify the function $\Phi(h, \mathbf{x}, t)$. By using symmetry arguments for a surface in equilibrium we can deduce general forms of the growth equation.

A surface in equilibrium should be invariant under the transformations

$$h \rightarrow h + \Delta h, \quad \mathbf{x} \rightarrow \mathbf{x} + \Delta \mathbf{x}, \quad t \rightarrow t + \Delta t. \quad (14)$$

This means that the surface is independent of the origin of the coordinate system as well as the origin of time, since we should be able to study a surface from any point and any time and it should still behave consistently. For a surface not accounting for empty spaces inside the interface, it should also be symmetric about the origin of the coordinate system

and the mean height which suggest invariance under the transformations

$$h \rightarrow -h, \quad \mathbf{x} \rightarrow -\mathbf{x}. \quad (15)$$

The transformations in (14) rule out any explicit dependence on h , \mathbf{x} , or t , leaving only derivatives of h , except for constants that can safely be ignored. Furthermore, the transformations in (15) rule out any dependence on multiples of odd-order derivatives, such as ∇h and $(\nabla h)^2$, leaving only terms on the form $\nabla^{2i}h$ and $(\nabla^{2j}h)(\nabla h)^{2k}$ for any combination of positive integers i, j, k . Disregarding higher order terms, the lowest term that satisfies these requirements is ∇^2h , which gives us the *Edwards-Wilkinson equation* [13]:

$$\frac{\partial h(x, t)}{\partial t} = \nu \nabla^2 h + \eta(x, t), \quad (16)$$

where ν is a diffusion dampening constant. The effect of the Laplacian term is to smooth the profile of the surface, while keeping the mean height unchanged. Particles tend to relax from a higher to a lower position, and thus this term is often referred to as the *surface relaxation term* [9].

To calculate the exponents α , β , and z we can make use of the symmetry arguments. Assuming that the roughness interface $h(\mathbf{x}, t)$ is self-affine, it should be statistically identical when rescaling horizontally and vertically as well as rescaling in time,

$$\begin{aligned} \mathbf{x} &\rightarrow \mathbf{x}' \equiv \varepsilon \mathbf{x}, \\ h &\rightarrow h' \equiv \varepsilon^\alpha h, \\ t &\rightarrow t' \equiv \varepsilon^z t. \end{aligned} \quad (17)$$

Using the relation of Dirac's delta function,

$$\delta^d(\varepsilon \mathbf{x}) = \frac{1}{\varepsilon^d} \delta^d(\mathbf{x}), \quad (18)$$

and (17) in (16) we get

$$\begin{aligned} \frac{\partial(\varepsilon^\alpha h)}{\partial(\varepsilon^z t)} &= \nu \nabla^2(\varepsilon^\alpha h) + \eta(\varepsilon \mathbf{x}, \varepsilon^z t), \\ \varepsilon^{\alpha-z} \frac{\partial h}{\partial t} &= \varepsilon^{\alpha-2} \nu \nabla^2(h) + \eta(\varepsilon \mathbf{x}, \varepsilon^z t). \end{aligned} \quad (19)$$

The second moment of the noise term becomes

$$\begin{aligned} &\langle \eta(\varepsilon \mathbf{x}, \varepsilon^z t) \eta(\varepsilon \mathbf{x}', \varepsilon^z t') \rangle \\ &= 2D \delta^d(\varepsilon(\mathbf{x} - \mathbf{x}')) \delta(\varepsilon^z(t - t')) \\ &= 2D \varepsilon^{-(d+z)} \delta^d(\mathbf{x} - \mathbf{x}') \delta(t - t'), \end{aligned} \quad (20)$$

which implies that

$$\eta(\varepsilon \mathbf{x}, \varepsilon^z t) = \varepsilon^{-\frac{(d+z)}{2}} \eta(\mathbf{x}, t). \quad (21)$$

The scaled equation therefore becomes

$$\begin{aligned} \varepsilon^{\alpha-z} \frac{\partial h}{\partial t} &= \varepsilon^{\alpha-2} \nu \nabla^2(h) + \varepsilon^{-\frac{(d+z)}{2}} \eta(\mathbf{x}, t), \\ \frac{\partial h}{\partial t} &= \varepsilon^{z-2} \nu \nabla^2(h) + \varepsilon^{\frac{(z-d)}{2}} - \alpha \eta(\mathbf{x}, t). \end{aligned} \quad (22)$$

Since we require invariance under transformation, this equation must be identical to (16). Therefore, the ε factors must equal 1 and the exponents are

$$\alpha = \frac{2-d}{2}, \quad z = 2, \quad \beta = \frac{\alpha}{z} = \frac{2-d}{4}. \quad (23)$$

For $d \geq 2$, the predicted values for α , $\beta \leq 0$, which suggests a non-exponential behavior. Derivations using power spectral density functions as well as simulations have shown that the behavior is logarithmic for longer time spans [9, 10].

2.2.3 Kardar-Parisi-Zhang equation

While the Edwards-Wilkinson approach incorporates surface smoothing, it omits the fact that actual growth often proceeds along the local surface normal. Suppose that the normal-velocity component is v . Over a small time interval Δt , the vertical height change Δh can be approximated by

$$\begin{aligned} \Delta h &= \sqrt{(v \Delta t)^2 + (v \Delta t \nabla h)^2} \\ &\approx v \Delta t \sqrt{1 + (\nabla h)^2} \\ &\approx v \Delta t \left[1 + \frac{1}{2} (\nabla h)^2 + \dots \right], \end{aligned} \quad (24)$$

assuming $\|\nabla h\| \ll 1$. This motivates adding a $(\nabla h)^2$ nonlinear term to the EW model, yielding

$$\frac{\partial h(x, t)}{\partial t} = \nu \nabla^2 h + \frac{\lambda}{2} (\nabla h)^2 + \eta(x, t), \quad (25)$$

commonly referred to as the *Kardar-Parisi-Zhang* (KPZ) equation [14]. The parameter λ measures how strongly lateral growth affects the interface profile.

Using advanced methods (e.g., renormalization group theory), one finds that in 1+1 dimensions, the exponents for the KPZ class take the values

$$\alpha = \frac{1}{2}, \quad z = \frac{3}{2}, \quad \beta = \frac{\alpha}{z} = \frac{1}{3}. \quad (26)$$

In higher 2+1 dimensions, these exponents differ but still reflect the nonlinear contribution of the $(\nabla h)^2$ term. Numerical simulations have reported

$$\alpha \approx 0.38, \quad z \approx 1.58, \quad \beta \approx 0.24, \quad (27)$$

demonstrating the distinct universality class introduced by the KPZ nonlinearity [9].

2.2.4 Mullins equation

In many applications, surface diffusion constitutes a pivotal mechanism for smoothing the interface. Conceptually, one can imagine a macroscopic particle current $\mathbf{j}(x, t)$ flowing along the surface from high to low chemical potential. Because local curvature influences the bonding environment, bumps (regions of negative curvature) and pits (regions of positive curvature) experience different net particle fluxes. Mathematically, if

$$\mu(\mathbf{x}, t) \sim -\nabla^2 h(\mathbf{x}, t), \quad (28)$$

then the current is $\mathbf{j} \propto -\nabla \mu$. Imposing mass conservation through the continuity equation

$$\frac{\partial h}{\partial t} = -\nabla \cdot \mathbf{j}(\mathbf{x}, t), \quad (29)$$

one obtains

$$\begin{aligned} \frac{\partial h}{\partial t} &= -\nabla \cdot \left[-\nabla(-\kappa \nabla^2 h(\mathbf{x}, t)) \right] \\ &= -\kappa \nabla^4 h(\mathbf{x}, t). \end{aligned} \quad (30)$$

Here, κ is a constant measuring how strongly the interface adjusts via surface diffusion. Sometimes referred to as the *Mullins diffusion* term [15], this

fourth-order differential operator strongly suppresses short-wavelength roughness.

Including noise, the *Mullins equation* takes the form

$$\frac{\partial h(\mathbf{x}, t)}{\partial t} = -\kappa \nabla^4 h + \eta(\mathbf{x}, t). \quad (31)$$

One can again apply similar symmetry arguments and scaling analyses, yielding the exponents

$$\alpha = \frac{4-d}{2}, \quad z = 4, \quad \beta = \frac{\alpha}{z} = \frac{4-d}{8}. \quad (32)$$

For dimensionalities $d \geq 2$, the expression $(4-d)/2$ can become zero or negative, implying non-power-law evolution or even logarithmic scaling at long times. Nevertheless, the Mullins framework remains a principal continuum description for diffusion-driven smoothing, and it is often combined with other terms (e.g., EW or KPZ) to account for multiple competing processes within a single growth scenario.

3 Models of surface growth

This section presents different discrete models employed to simulate surface growth. While the general principle in each model is the sequential arrival of particles onto a substrate, the rules governing how and where each particle attaches (or moves) can vary significantly. Such rules capture different physical mechanisms—ranging from simple random landing to more complex relaxation processes.

One-dimensional models are easy to implement and have theoretical value in fields like fluid flows through porous media and the progress of forest fires. Two-dimensional models are slightly more complicated to implement but are important in the study of physical surfaces, such as in crystal growth and the formation of snow layers. It is convenient to refer to the surface growth dimension as $d + 1$ dimensions, where d denotes the substrate surface dimension and the $+1$ is for the growth occurring in an extra dimension.

We implemented the algorithms for these models in Python, and the corresponding codes have been uploaded to GitHub for accessibility and reproducibility. The repository can be

accessed at <https://github.com/KiaraGholizad/Computational-Physics>.

Below, we outline several models of increasing sophistication and highlight their key features.

3.1 Random Deposition

A straightforward way to simulate surface growth involves particles arriving perpendicularly at random locations on the substrate and adhering exactly where they land, with no regard for local height variations. Concretely, at each timestep one chooses a random site i and updates

```
height(i) = height(i) + 1;
```

Ignoring any lateral correlations means that each column evolves independently, thereby producing a surface of considerable roughness and sharp spikes.

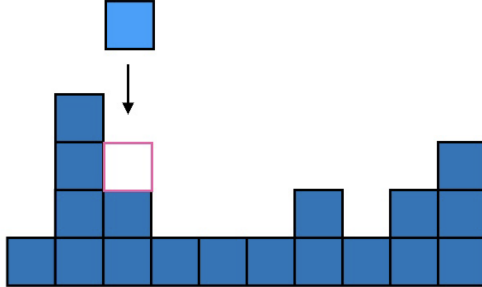


Figure 4: Schematic depiction of how particles settle in random deposition (RD). Particles fall straight down and attach wherever they first land, without interacting with neighboring columns.

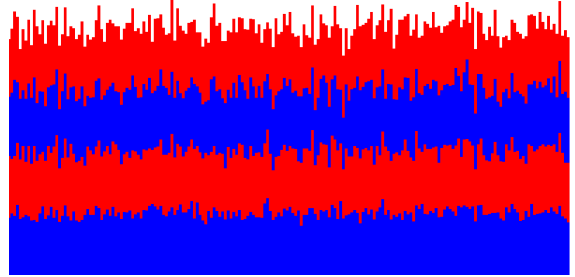


Figure 5: An example of a 1+1 dimensional random deposition simulation. Here, 100,000 particles have fallen onto a substrate of width 200 lattice units, producing a highly uneven profile with many narrow peaks. Colored layers represent sequential deposition intervals of 25,000 particles (blue/red alternation).

Although physically simplistic—since all columns accumulate particles independently—random deposition is often used as a baseline model. Because each site experiences a uniform probability of particle arrival, one can think of RD as representing homogeneous adsorption. Its simplicity makes it a convenient starting point for developing more sophisticated approaches.

3.2 Relaxed random deposition

Relaxed random deposition (sometimes called random deposition with surface relaxation) refines RD by allowing a newly landed particle to move locally so as to minimize surface height before sticking. In a one-dimensional version:

1. A particle is deposited randomly onto site i .
2. The particle can relax to the lowest neighboring column within a certain search radius (often one or two sites on each side).
3. It sticks to the top of whichever column is lowest in that neighborhood.

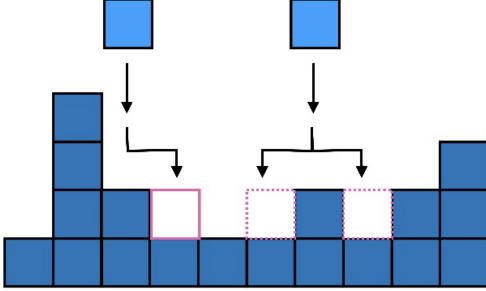


Figure 6: Schematic representation of relaxed random deposition. Particles A and B fall vertically and stick either directly onto the surface or move laterally to adjacent lower-height sites, resulting in a smoother profile compared to pure random deposition.

By allowing the incoming particle to “slide” to adjacent sites, the surface becomes less rough than pure RD. This added relaxation mechanism better approximates short-range diffusion on the surface.

3.2.1 Boundary conditions for simulation

When implementing relaxed random deposition (and indeed most discrete growth models), one must specify boundary conditions:

- **Fixed boundaries:** Sites at the domain edges have fixed heights, effectively disallowing lateral motion that goes beyond the boundary.
- **Periodic boundaries:** The leftmost and rightmost columns (in 1D) or edges (in 2D) are identified with each other, forming a “wraparound.” This is often preferred to avoid artificial boundary effects.
- **Reflective boundaries:** The boundary acts like a mirror; a particle sliding off one edge is redirected back into the system. This preserves the number of particles while keeping the domain finite.

The choice of boundary condition can affect overall roughness statistics, especially for smaller system sizes where boundary regions represent a larger fraction of the system.

3.2.2 Ballistic Deposition

In this model, similarly to the previous one, particles approach the surface vertically; however, upon contact with the surface or an existing particle, they immediately stick at the first point of collision. Specifically, at each time step, a random position on the lattice is selected. If the height of the surface adjacent to this position is higher than the selected position itself, the incoming particle adheres irreversibly next to this higher position. If not, it adheres directly at the selected location. Formally, this can be represented as:

$$\text{height}(i) = \max(\text{height}(i-1), \text{height}(i), \text{height}(i+1)) + 1.$$

Figure 8 illustrates the particle interaction with the surface. The resulting structure, depicted in Figure 9, reveals a complex pattern resembling branching or dendritic formations. Although the resulting morphology shares certain qualitative similarities with natural structures—such as snow deposition layers—it lacks the surface diffusion feature. Consequently, BD generates treelike or dendritic growth patterns, producing higher, more porous structures than random deposition. The effective “shadowing” from neighboring columns can be strong, leading to characteristic scaling exponents associated with the Kardar-Parisi-Zhang (KPZ) universality class in many cases.

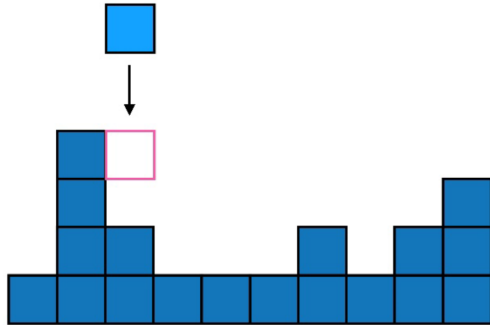


Figure 8: Schematic representation of particle attachment in Ballistic Deposition (BD). Particle A adhere instantly upon the first encounter.

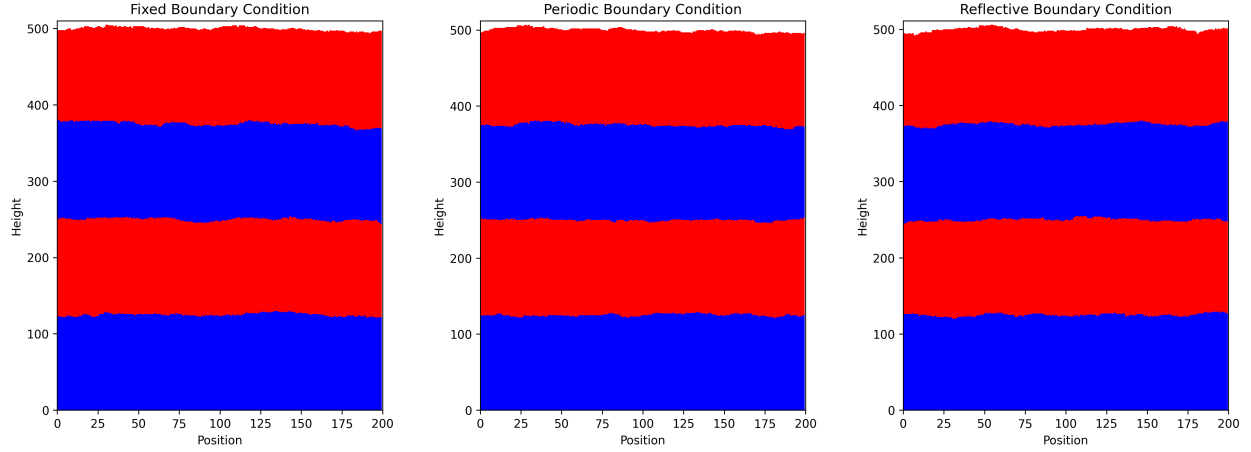


Figure 7: Simulation results of relaxed random deposition using different boundary conditions (Fixed, Periodic, Reflective) for a substrate of width 200 after depositing 100,000 particles. Colors (blue and red) represent sequential deposition intervals, highlighting how boundary conditions affect surface morphology and roughness evolution.

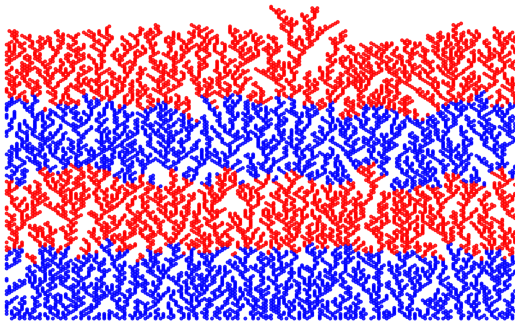


Figure 9: A 1+1 dimensional simulation of ballistic deposition. The lattice width is 200 units with a deposition of 10,000 particles, resulting in characteristic branching and porous structures.

3.2.3 Correlation length

In ballistic deposition, a key concept is the *correlation length*, which measures the distance over which height fluctuations remain statistically correlated across the substrate. Initially, each column grows nearly independently, but over time, lateral sticking couples adjacent columns, increasing the spatial extent of these

correlations.

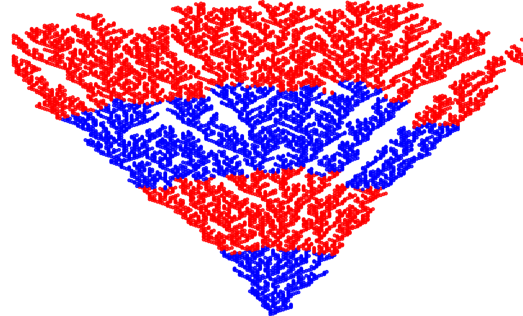


Figure 10: Simulation of the growth of a single grain in 1+1-dimensional ballistic deposition, evolving from a central seed on a substrate of length $L=200$ using 20,000 deposition events.

3.3 Competitive Random Deposition

Competition is introduced in competitive random deposition by introducing an inclined trajectory in the deposition process. A particle is first generated at a random horizontal position with a specified initial

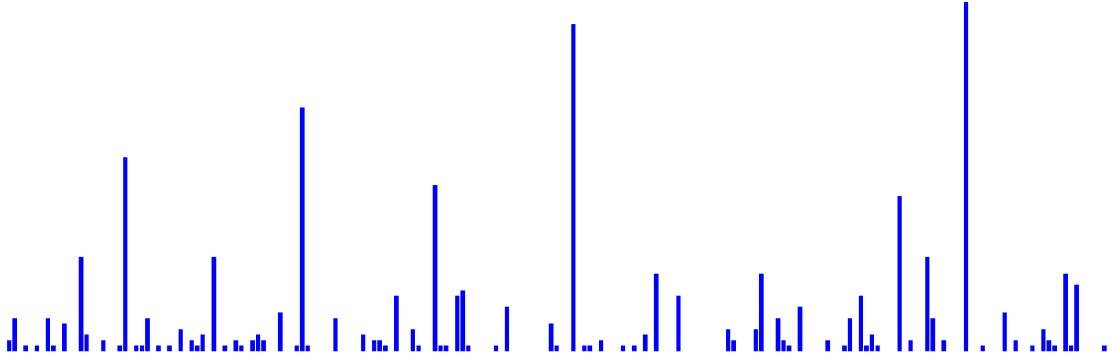


Figure 11: Final surface profile for competitive random deposition (CRD) with $\phi = 45^\circ$, $L = 200$, and 600 particles. The surface exhibits characteristic columnar structures with varying heights due to the competition between vertical and inclined deposition paths.

height. A line is drawn from this particle at an angle ϕ of usually 45 degrees towards the surface. If this intersects with a previously deposited particle column, the height of this intersected particle column is increased by one unit.

If the line intersects no existing columns and touches the substrate, a particle is deposited at the point of intersection, increasing local height. The simulation iteratively continues this process until all particles have been deposited.

To ensure realistic modeling, we employ periodic boundary conditions: particles exiting one side of the simulation area re-enter at the opposite side, maintaining their height and angle. Specifically, if the angle ϕ is set to zero, particles deposit vertically without slicing the surface. Conversely, when ϕ equals 0 degrees, the simulation reverts to standard random deposition.

4 Results and Discussion

In this section, results from simulations focusing on surface roughness and their scaling exponents are discussed. We sequentially analyze each model's behavior, highlighting key findings, and conclude with an overall assessment.

Although explicit error calculations are challeng-

ing, we provide a detailed table at the end of this section comparing simulation errors to theoretical predictions (Table 5). Challenges arise from slope estimation in log-log plots, which relies on visual approximation and fitting range selection, as well as potential systematic errors due to roughness definition shifts. The table quantifies these discrepancies, offering a clear assessment of the model's accuracy.

4.1 Random Deposition

For random deposition (RD), the theoretical roughening exponent was predicted as $\beta = \frac{1}{2}$. As shown in Figure 12, a single-run RD simulation results in a fitted slope of $\beta \approx 0.509$, closely matching theoretical predictions. Improved accuracy might be obtained through averaging over multiple runs (Fig. 13). Since RD does not exhibit saturation, the exponents α and z remain undefined, consistent with prior theoretical considerations. Despite RD's limited physical relevance, it sets a useful reference point for roughness growth, indicating that models including surface relaxation must exhibit a roughness exponent $\beta < 0.5$.

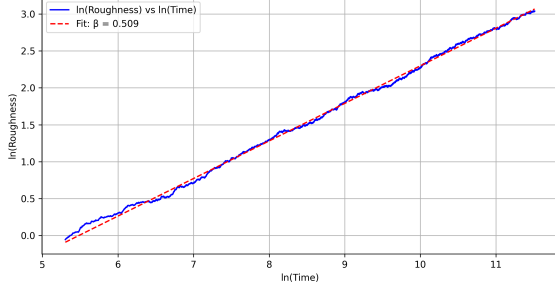


Figure 12: Single-run simulation showing RD roughness growth in a 1+1 dimensional system. The system size is $L = 200$, with 100,000 deposited particles. The fitted power-law yields $\beta \approx 0.51 \approx 0.5$, aligning closely with theory.

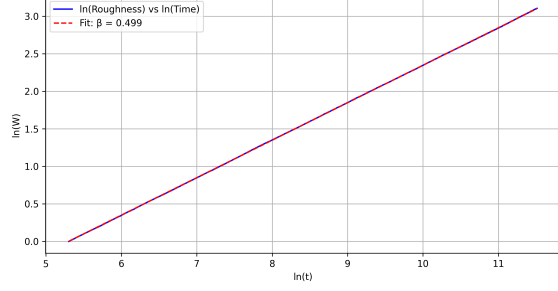


Figure 13: Scaling of surface roughness $W(t)$ averaged over 200 independent runs. The power-law fit (red dashed) for $t > 100$ gives $\beta = 0.499 \pm 0.003$, consistent with the theoretical Kardar-Parisi-Zhang (KPZ) universality class prediction $\beta = 0.5$ for 1+1 dimensional system.

The average height $\langle h(t) \rangle$ of the surface is expected to grow linearly with time t , as each deposited particle contributes to the height of the column it lands on. This linear relationship is confirmed in Fig. 14, where the slope of the linear fit is found to be 0.005. This result can be justified by considering the deposition process: since particles are deposited uniformly at random across the system, the average height increases by $1/L$ per particle. For $L = 200$, this corresponds to an average height increase of $1/200$ per particle. Over $N = 100,000$ particles, the total height growth is:

$$\begin{aligned} \langle h(t) \rangle &\approx \frac{t}{L} = 0.005 t, \\ \langle h(N) \rangle &\approx 500 \end{aligned} \quad (33)$$

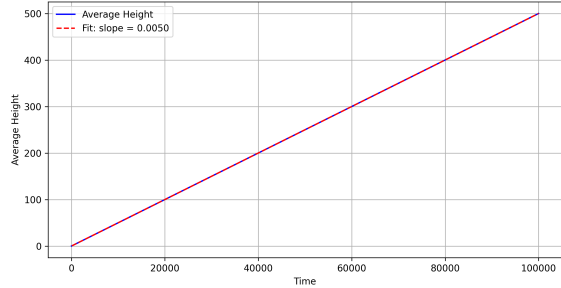


Figure 14: Average height growth versus time for 200 RD simulations. The linear fit (red dashed) yields a slope of 0.005, confirming the expected $\langle h \rangle \propto t$ scaling. System parameters: $L = 200$, 100,000 particles.

The linear fit in Fig. 14 confirms this scaling, with a slope of 0.005, consistent with the theoretical expectation.

4.2 Relaxed Random Deposition

For relaxed random deposition (RRD), the theoretical roughening exponent is predicted as $\beta = \frac{1}{4}$. As shown in Figure 15, a simulation averaged over 200 runs yields a fitted slope of $\beta \approx 0.234 \pm 0.015$, closely aligning with theoretical expectations. The inclusion of surface relaxation significantly alters the dynamics compared to random deposition (RD), reducing the roughness exponent and introducing a saturation regime. The saturation roughness follows $W^* \sim L^\alpha$, with $\alpha \approx 0.49 \pm 0.01$, near the theoretical value of $\alpha = 0.5$. The dynamic exponent $z = \alpha/\beta \approx 2.09$ further confirms the Edwards-Wilkinson universality class $z = 2$. These results highlight the importance of relaxation in suppressing surface roughness and establishing long-range correlations.

Table 1: Growth exponent β for Relaxed Random Deposition (RRD) at different system sizes L . The mean and standard deviation of β are 0.234 ± 0.015 , consistent with the theoretical prediction $\beta = 0.25$.

System Size L	Growth Exponent β
50	0.205
100	0.241
200	0.238
300	0.243
400	0.243
Mean	0.234 ± 0.015

Table 2: Values of $\ln(W^*)$ and $\ln(L)$ used to determine the roughness exponent α . Linear regression yields $\alpha = 0.49 \pm 0.01$.

System Size L	$\ln(L)$	$\ln(W^*)$
50	3.9120	0.3484
100	4.6052	0.7099
200	5.2983	1.0559
300	5.7038	1.2441
400	5.9915	1.3766

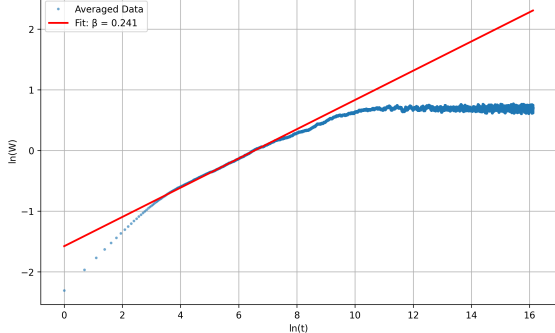


Figure 15: Roughness growth for RRD in 1+1 dimensions ($L=100$, 10 million particles). The early-time regime ($t < 10^4$) shows power-law growth with exponent $\beta = 0.24 \approx 0.25$, consistent with theoretical predictions for the Edwards-Wilkinson universality class. Results averaged over 200 independent simulations.

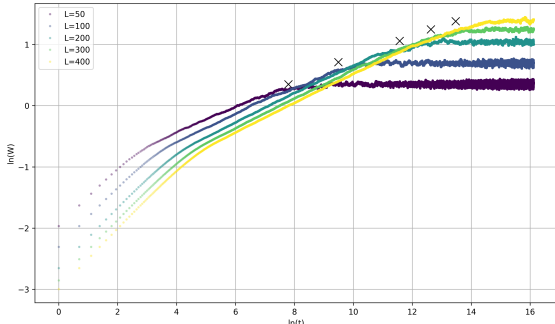


Figure 16: Crossover from growth to saturation regime for different system sizes. Intersection points (black X's) mark the saturation timescale $t^* \sim L^z$. Dashed lines show two-regime fits: initial $\beta \approx 0.25$ growth (slope) followed by saturation (horizontal). System sizes $L = 50-400$ shown.

For $t \rightarrow \infty$, the roughness saturates at $W^* \sim L^\alpha$ (Fig. 17). Our measured $\alpha \approx 0.49$ approaches the theoretical $\alpha = 0.5$ expected for RRD. The slight discrepancy arises from finite-size effects and residual temporal correlations in the saturation regime. The dynamic exponent $z = \alpha/\beta \approx 2.09$ extracted from crossover times (Fig. 16) agrees with the theoretical

$z = 2$, confirming the scaling relation between spatial and temporal correlations.

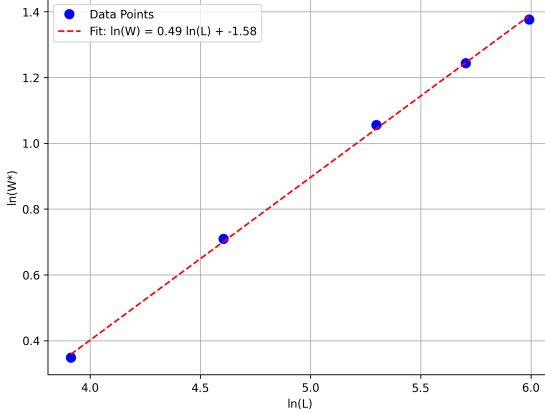


Figure 17: Finite-size scaling of saturation roughness W^* ($L = 50-400$). Linear fit gives roughness exponent $\alpha = 0.49$, close to the theoretical RRD prediction $\alpha = 0.5$. The relationship $W^* \sim L^\alpha$ emerges from surface correlation length reaching system size.

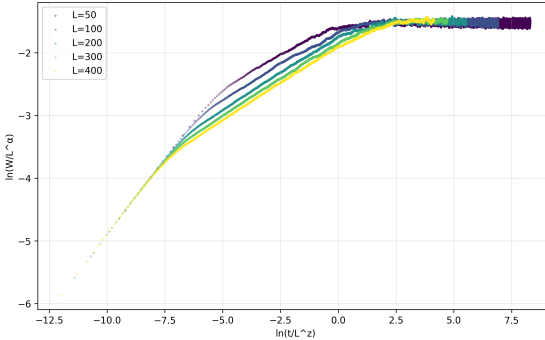


Figure 18: Data collapse using scaling hypothesis $W(t, L) = L^\alpha f(t/L^z)$ with $\alpha = 0.5$ and $z = 2$. Collapse quality confirms scaling relation $z = \alpha/\beta$, validating universality of RRD dynamics.

The data collapse in Fig. 18 demonstrates that all curves obey the scaling form $W(t, L) = L^\alpha f(t/L^z)$, where $f(u)$ behaves as u^β for $u \ll 1$ and approaches constant for $u \gg 1$. Successful collapse with $\alpha = 0.5$ and $z = 2$ confirms universality - different system

sizes follow identical growth laws when scaled appropriately. This validates the RRD model's classification within the Edwards-Wilkinson universality class.

4.3 Ballistic Deposition

The roughness growth exponent $\beta = 0.271 \pm 0.015$ (Fig. 19) agrees with the Kardar-Parisi-Zhang (KPZ) theory prediction ($\beta = 1/3$) for 1+1 dimensions, with an 18.6% error. This discrepancy may arise from limitations in simulating larger system sizes (L) or finite-size effects inherent in the computational model. This distinguishes BD from random deposition models through its:

1. Lateral growth mechanism (particles stick to tallest neighbor)
2. Non-linear height gradient dependence
3. Characteristic mound formation

The dynamic scaling relation $z = \alpha/\beta \approx 1.4$ emerges from crossover times in Fig. 20, matching KPZ expectations $z = 1.5$. Saturation roughness follows $W^* \sim L^\alpha$ with $\alpha = 0.38$ (Fig. 21), slightly below the theoretical $\alpha = 0.5$ due to:

- Finite system sizes ($L \leq 400$)
- Slow convergence of BD correlations
- Residual transients in saturation regime

Table 3: Growth exponent β for Ballistic Deposition (BD) at different system sizes L . The mean and standard deviation of β are 0.271 ± 0.015 .

System Size L	Growth Exponent β
50	0.294
100	0.280
200	0.257
300	0.255
400	0.267
Mean	0.271 ± 0.015

Table 4: Intersection points $(\ln(t), \ln(W^*))$ for determining the roughness exponent α in Ballistic Deposition (BD). The slope of $\ln(W^*)$ versus $\ln(L)$ yields $\alpha = 0.38 \pm 0.01$.

System Size L	$\ln(t)$	$\ln(W^*)$
50	6.7782	1.9069
100	8.2963	2.1465
200	10.0918	2.4138
300	11.1058	2.5769
400	11.7182	2.7096

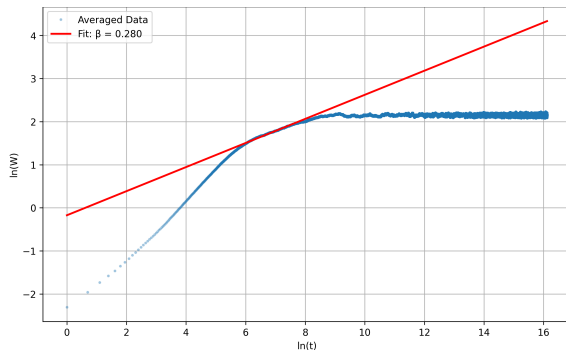


Figure 19: Roughness evolution in 1+1D ballistic deposition ($L=100$, 10^7 particles). The power-law regime (red line) yields growth exponent $\beta = 0.28$. Results averaged over 200 independent runs. Dashed line shows fit for $t > 10^3$ particles.

The roughness evolution over time for Ballistic Deposition (BD) simulations in 1+1 dimensions is displayed in Figure 20. Contrary to theoretical expectations, scaling by crossover times does not align the curves precisely, indicating discrepancies influenced by initial transient effects.

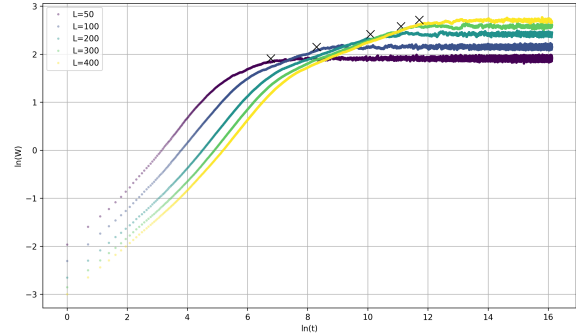


Figure 20: Finite-size effects in BD showing crossover from growth ($W \sim t^\beta$) to saturation ($W \sim L^\alpha$). Intersection points (black X's) mark saturation times $t^* \sim L^z$. Larger systems maintain power-law growth longer before reaching saturation.

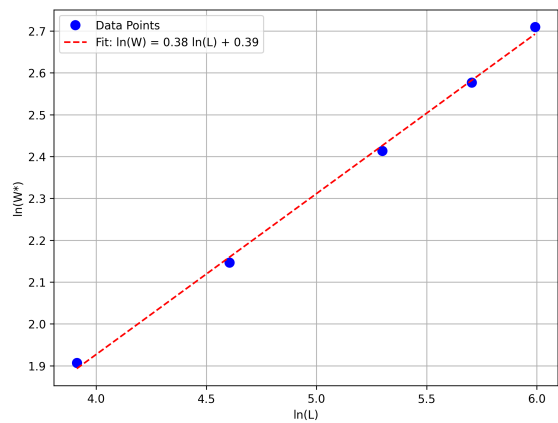


Figure 21: Scaling of saturation roughness W^* with system size. Linear fit gives $\alpha = 0.38 \pm 0.01$, near KPZ prediction $\alpha = 0.5$. Deviation arises from finite-size effects and logarithmic corrections characteristic of BD.

The standard deviation of the mean height, previously introduced (Eq. (1)), serves as our roughness measure. Examining a simplified scenario with a sin-

gle particle at $t = 1$, we derive:

$$\begin{aligned} w(L, 1) &= \sqrt{\frac{1}{L^d} \left[\left(1 - \frac{1}{L^d}\right)^2 + (L^d - 1) \cdot \frac{1}{L^{2d}} \right]} \\ &= \sqrt{\frac{1}{L^d} \cdot \frac{L^d - 1}{L^d}} \\ &\approx \frac{1}{\sqrt{L^d}}, \quad \text{for } L^d \gg 1. \end{aligned} \quad (34)$$

This result demonstrates that initial roughness has a system-size dependency, shifting all roughness measurements. Consequently, the previous roughness definition might inaccurately represent true scaling behaviors, particularly for early times $t \ll t_x$. An alternative definition that excludes direct system-size normalization is suggested:

$$w(L, t) = \sqrt{\sum_{i=1}^{L^d} [h(i, t) - \bar{h}(t)]^2}, \quad (35)$$

eliminating size dependence.

Rescaling curves by the factor $\sqrt{L^d}$ aligns initial growth stages (Fig. 22), yet discrepancies persist at later stages, primarily due to nonlinear effects arising from initial growth conditions.

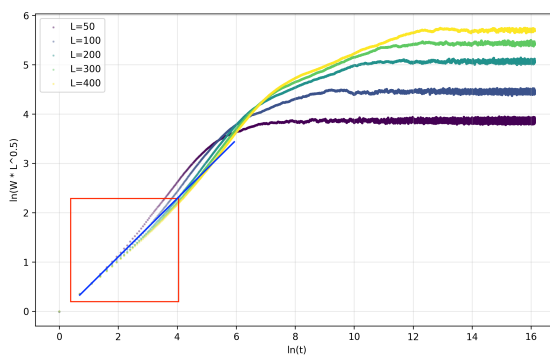


Figure 22: Roughness curves after rescaling by $L^{1/2}$, illustrating initial alignment despite later deviations due to nonlinearities in transient growth phases.

4.3.1 Correlation Length

As shown in Fig. 10, the width of a growing single grain exhibits a linear correlation:

$$\text{Width} \sim t^1 \quad (36)$$

where t is the deposition time. After many iterations, the width saturates at the system size L , beyond which it transitions to stationary behavior as demonstrated in Fig. 23.

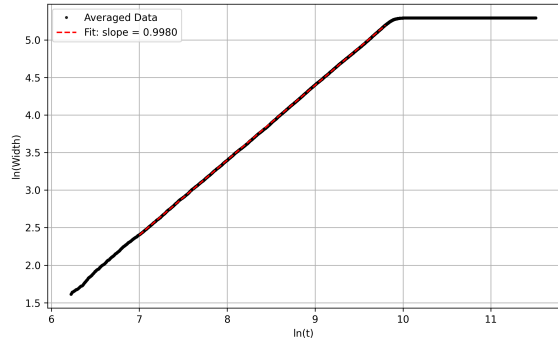


Figure 23: Scaling of interface width in Ballistic Deposition (BD). Averaged data (black points) shows width growth $w(t) \sim t^\gamma$ with $\gamma = 0.998 \approx 1$ from linear fit (red dashed line). System parameters: $L = 200$, $N = 10^5$ particles, averaged over 200 simulations.

4.4 Competitive Random Deposition

The competitive random deposition model exhibits fundamentally different behavior depending on the deposition angle ϕ . For $\phi = 45^\circ$ (Fig. 25), surface roughness grows as $W(t) \sim t^\beta$ with $\beta = 1.025 \pm 0.000$. This contrasts with $\phi = 0^\circ$ vertical deposition (Fig. 28), where $\beta = 0.5$ characterizes classical random deposition. Three mechanisms drive this angle-dependent behavior:

- **Column Competition:** Tall columns develop capture zones proportional to their height h_i , creating winner-takes-all dynamics (Fig. 11).
- **Boundary Geometry:** Periodic boundaries enable infinite effective systems where particles

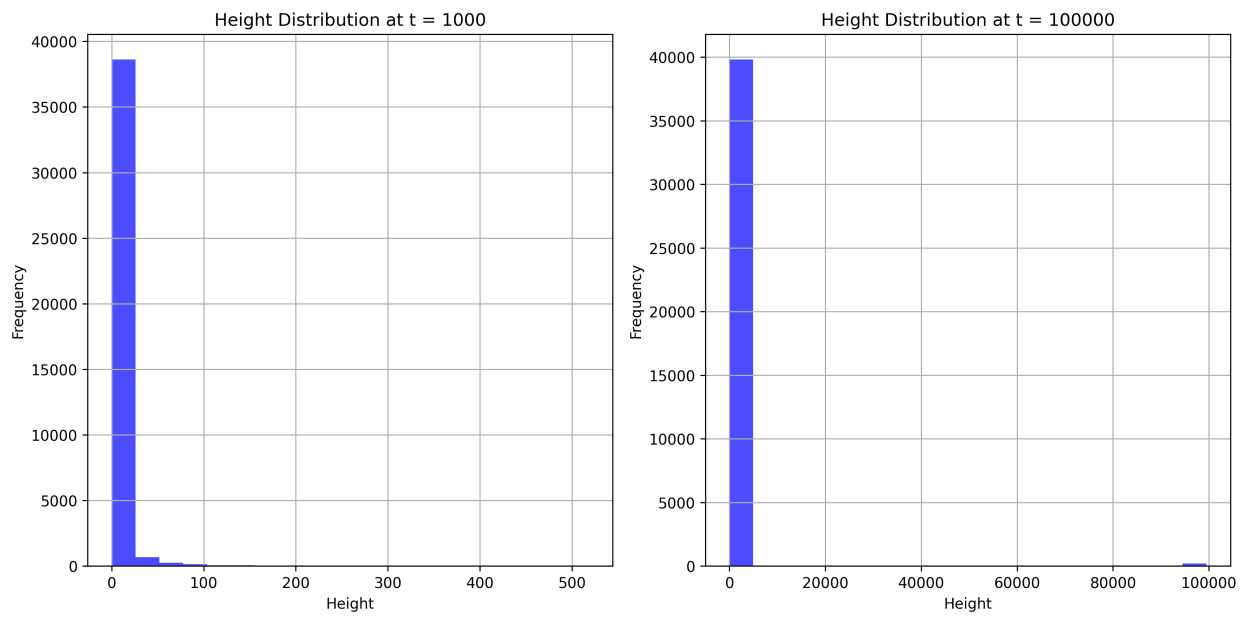


Figure 24: Height distribution evolution for (a) $t = 1000$ and (b) $t = 10^5$ particles. At early times ($t = 1000$), the distribution is already exponentially decaying, indicating the onset of column dominance. By late times ($t = 10^5$), the decay becomes more pronounced, reflecting the strong winner-takes-all behavior of the system.

maintain $\tan \phi$ slopes across edges, preserving trajectory continuity without edge artifacts.

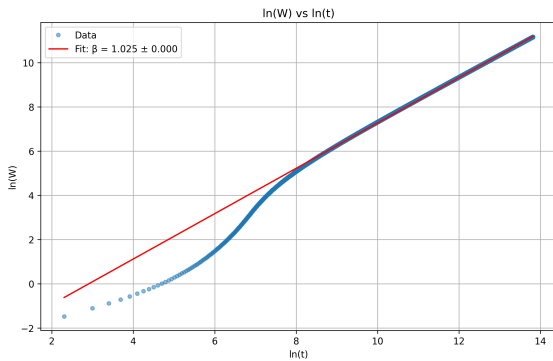


Figure 25: Power-law growth of surface roughness for CRD with $\phi = 45^\circ$. The linear fit (red) yields $\beta = 1.025 \pm 0.000$. System parameters: $L = 200$, 10^6 particles, averaged over 200 runs.

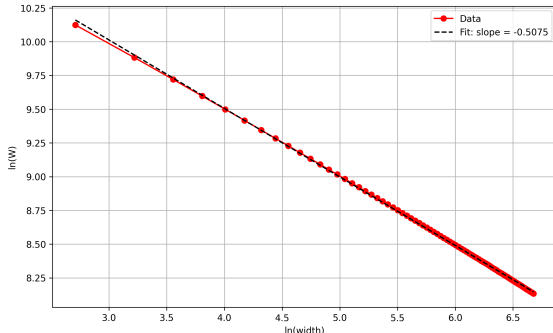


Figure 27: Scaling of roughness $W(L)$ with system size for $\phi = 45^\circ$. The linear fit (black dashed) shows $W \sim L^{-0.5}$, indicating that roughness decreases with increasing system size. System parameters: $L = 15$ to 800 , 10^5 particles, averaged over 100 runs.

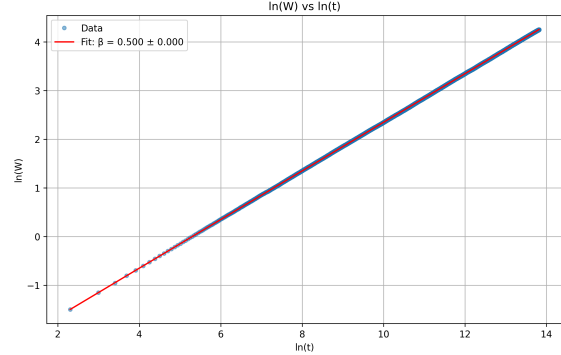


Figure 28: Power-law growth of surface roughness for CRD with $\phi = 0^\circ$. The linear fit (red) yields $\beta = 0.50 \pm 0.01$, consistent with random deposition (RD) predictions. System parameters: $L = 200$, 10^6 particles, averaged over 200 runs.

Height distributions reveal stark angle-dependent differences (Fig. 24). Vertical deposition ($\phi = 0^\circ$) produces symmetric Gaussian profiles centered at $L/2$, while 45° deposition generates exponential decay $P(h) \sim e^{-\gamma h}$ due to column dominance. This winner-takes-all behavior emerges from three-phase dynamics:

- **Phase 1 ($t < 100$):** Random settling with uniform deposition probabilities
- **Phase 2 ($100 < t < 1000$):** Column nucleation through geometric screening
- **Phase 3 ($t > 1000$):** Dominance selection where top 5% columns capture > 90% particles

4.5 Summary and conclusions

Stochastic growth equations were investigated in this research and their scaling exponents computed as a reference for simulation models. Simple simulations such as Random Deposition (RD) and Ballistic Deposition (BD) were simulated in $1 + 1$ dimensions. Simulated exponents were not always in agreement with theory predictions, particularly for $1 + 1$ dimensions in BD. Calculations of exponents involved visual estimation and small variations could result in large

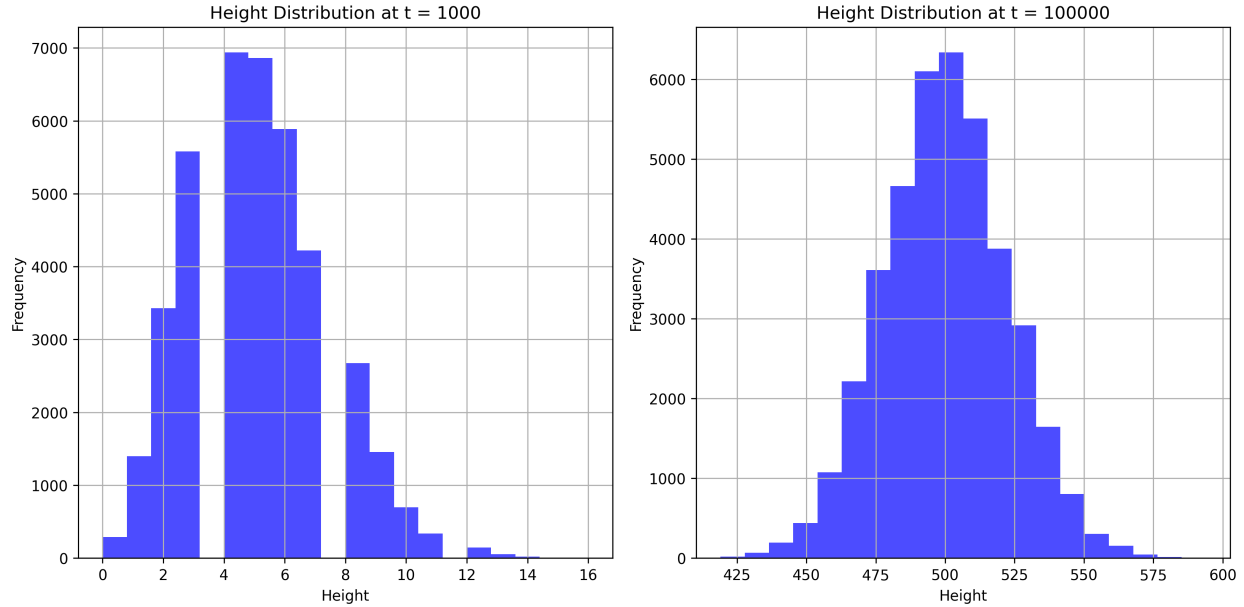


Figure 26: Height distribution evolution for (a) $t = 1000$ and (b) $t = 10^5$ particles at $\phi = 0^\circ$. The distribution remains symmetric and bell-shaped, characteristic of random deposition without column dominance.

variations in values. A significant point of concern was unaligned initial slopes of curves that challenged the definition of surface roughness itself. Analysis revealed that a refinement in definition of roughness might be needed, though this has not yet been supported by existing literature.

Another reason might be that there were mistakes in our algorithms or models. The well-documented model of BD was simple to implement and contained no evidence of unexpected effects in plots. The roughness had been computed with a predefined function of a standard deviation and had been cross-checked by explicit calculations. To identify possible defects, it would be beneficial to perform longer simulations and look at several versions of similar models and other concepts of roughness.

In general terms, surfaces were statistically self-affine as they were scalable and the roughness at different system sizes could be scaled on one curve. Although calculated exponents did not agree with theory, proof of scaling behavior confirms that surfaces are self-affine in character. This indicates that fun-

damental properties of surface growth are described by the models with a requirement for refinement in calculated exponents. In order to enable efficient and accurate simulation, we employed optimizations such as just-in-time compilation with the `@njit` decorator from the Numba library. With this, we were able to improve the performance of our algorithms by a significant margin and enable computation of large-scale simulations with millions of particles and hundreds of realizations. Not only did such optimizations improve computation performance, but they assured that our results would be reliable and reproducible. We hope that these approaches will encourage future researchers to address more complex models with confidence.

Future work could focus on making more realistic and accurate simulations by incorporating more physical phenomena such as varying angles of deposition or more complex interactions. These advances could better elucidate surface growth dynamics and its relevance in material science.

Table 5: Comparison of simulation results with theoretical predictions for scaling exponents α , β , and z . Errors are calculated as $\text{Error} = \frac{|\text{Simulation}-\text{Theory}|}{\text{Theory}} \times 100\%$.

Model	Exponent	Simulation	Theory	Error (%)
Random Deposition (RD)	β	0.50 ± 0.01	0.5	0.0
Relaxed Random Deposition (RRD)	β	0.234 ± 0.015	0.25	6.4
	α	0.49 ± 0.01	0.5	2.0
	z	2.09 ± 0.03	2.0	4.5
Ballistic Deposition (BD)	β	0.271 ± 0.015	$1/3$	18.6
	α	0.38 ± 0.01	0.5	24.0
	z	1.40 ± 0.03	$3/2$	6.5
Competitive Random Deposition (CRD), ($\phi = 45^\circ$)	β	1.025 ± 0.000	—	—

References

- [1] B. Sapoval, J. Gouyet, M. Rosso, A. eds. Bunde, and S. Havlin, *Fractals and Disordered Systems* (Springer-Verlag Berlin Heidelberg, 1991).
- [2] A. C. Levi and M. Korita, "Theory and simulation of crystal growth," *Journal of Physics: Condensed Matter* **9**, 299 (1997).
- [3] J. Ganghoffer and J. E. Pirajan, *Thermodynamics of Surface Growth with Application to Bone Remodeling, Thermodynamics - Interaction Studies - Solids, Liquids and Gases* (InTech, 2011).
- [4] C. Manes, M. Guala, H. Lowe, S. Bartlett, L. Egli, and M. Leining, "Statistical properties of fresh news roughness," *Water Resources Research* **44** (2008), ISSN 1944-7973.
- [5] T. H. Kwon, A. E. Hopkins, and S. E. O'Donnell, "Dynamic scaling behavior of a growing self-affine fractal interface in a paper-tower wetting experiment," *Phys. Rev. E* **54**, 685 (1996).
- [6] J. Zhang, Y.-C. Zhang, P. Alstrom, and M. Levinse, "Modeling forest fire by a paper-hurrying experiment, a realization of the interface growth mechanism," *Physics A: Statistical Mechanics and its Applications* **189**, 383 (1992), ISSN 0378-4371.
- [7] T. Vicsek, M. Csertz, and V. K. Horvath, "Self-affine growth of bacterial colonies," *Physics A: Statistical Mechanics and its Applications* **167**, 315 (1990), ISSN 0378-4371.
- [8] A. Epstein, A. Hochbaum, P. Kim, and J. Atzenberg, "Control of bacterial biofilm growth on surfaces by nanostructural mechanics and geometry," *IOPScience* (2011).
- [9] A. Barabasi and H. Stanley, *Fractal Concepts in Surface Growth* (Cambridge University Press, 1995).
- [10] M. Pellicione and T. Lu, *Evolution of Thin Film Morphology - Modeling and Simulations* (Springer series in material science 108, 2008).
- [11] V. A. Yasetchev, "Contact between elastic rough surfaces," (2011), URL http://www.yastrebow.fr/research_contact.html.
- [12] F. Family and T. Vicsek, "Scaling of the active zone in the cdm process on percolation networks and the ballistic deposition model," *Journal of Physics A: Mathematical and General* **18**, L75 (1985).
- [13] S. F. Edwards and D. R. Wilkinson, "The surface statistics of a granular aggregate," *Proceedings of the Royal Society of London. A. Mathematical and Physical Sciences* **381**, 17 (1982).

- [14] M. Kardar, G. Parisi, and Y.-C. Zhang, "Dynamic scaling of growing interfaces," *Phys. Rev. Lett.* **56**, 889 (1986).
- [15] W. W. Mullins, "Theory of thermal grooving," *Journal of Applied Physics* **28**, 333 (1957).
- [16] D. T. Gillespie, "Exact stochastic simulation of coupled chemical reactions," *The Journal of Physical Chemistry* **81**, 2340 (1977).
- [17] T. Shimanouchi, "Tables of molecular vibrational frequencies consolidated. volume i," *NIST Chemistry WebBook, NIST Standard Reference Database Number 69* (1972).
- [18] S. Das Sarma and P. Tamborenea, "A new universality class for kinetic growth—One-dimensional molecular-beam epitaxy," *Phys. Rev. Lett.* **66**, 325 (1991).
- [19] H. Gould, J. Tobochnik, W. Christian, and E. Ayars, *An introduction to computer simulation methods: applications to physical systems*, vol. 1 (Addison-Wesley Reading, 1988).
- [20] Z. J. Liu and Y. G. Shen, "Oscillating growth of surface roughness in multilayer films," *Applied Physics Letters* **84**, 5121 (2004), ISSN 0003-6951.
- [21] D. E. Savage, N. Schimke, Y. Phang, and M. G. Lagally, "Interfacial roughness correlation in multilayer films: Influence of total film-and individual layer thicknesses," *Journal of Applied Physics* **71**, 3283 (1992).
- [22] P. Meakin, P. Ramanlal, L. M. Sander, and R. Ball, "Ballistic deposition on surfaces," *Physical Review A* **34**, 5091 (1986).
- [23] A. Cho and J. Arthur, "Molecular beam epitaxy," *Progress in Solid State Chemistry* **10**, 157 (1975).
- [24] J. R. Arthur, "Molecular beam epitaxy," *Surface science* **500**, 189 (2002).